

Chapter 15

Neutron Stimulated Emission Computed Tomography: A New Technique for Spectroscopic Medical Imaging

A. J. Kapadia

Abstract Neutron stimulated emission computed tomography (NSECT) is being developed as a new medical-imaging technique to quantify spatial distributions of elements in a sample through inelastic scattering of fast neutrons and detection of the resulting gamma rays. It has the potential to diagnose several disorders in the human body that are characterized by changes in element concentration in the diseased tissue. NSECT is sensitive to several naturally occurring elements in the human body that demonstrate concentration changes in the presence of diseases. NSECT, therefore, has the potential to noninvasively diagnose such disorders with radiation dose that is comparable to other ionizing imaging modalities. This chapter discusses the development and progress of NSECT and presents an overview of the current status of the imaging technique.

Keywords Inelastic scatter · Medical imaging · NSECT · Neutron imaging · Spectroscopy · Tomography

15.1 Introduction and Background

Neutron spectroscopic techniques have been widely used in medical and biomedical research to detect the presence of elements in the body. Techniques, such as instrumental neutron activation analysis (INAA), prompt-gamma neutron activation analysis (PGNAA), and delayed neutron activation analysis (DNAA), have been used since the 1960s to identify elements in healthy and diseased tissue, and techniques based on inelastic scattering of fast neutrons have been used frequently in body composition studies to measure whole body carbon and oxygen content.

The use of NAA techniques for medical applications was first reported in 1964 by Anderson et al. [1] for measurement of sodium in the body. Between

A.J. Kapadia (✉)

Duke Advanced Imaging Laboratories, Department of Radiology, Duke University Medical Center, Durham, NC 27705, USA
e-mail: anuj.kapadia@duke.edu

1968 and 1972, Chamberlain reported the measurement of body calcium and sodium in the body [2–4] and described techniques for whole-body NAA [5–7] and pulsed NAA [8]. In 1971, Cohn and Dombrowski reported the measurement of calcium, sodium chloride, nitrogen, and phosphorus in the human body through *in vivo* NAA [9]. Since then, NAA and PGNAA have been used for a variety of applications, such as the measurement of nitrogen [10], carbon and oxygen [11], cadmium [12], and manganese [13] in the body and in trace element research to identify cancerous tissue [14–17]. The development of NAA has been documented in several review articles [18–21], which the reader may refer to.

Inelastic neutron scatter analysis (INSA) using fast neutrons was initially reported by Kyere et al. in 1982 [22], who used 14 MeV neutrons from a (d,T) sealed-tube neutron generator to determine whole body carbon content as a measure of energy expenditure in the body. Following this experiment, Kehayias et al. reported methods to determine fat content in the body through measurement of whole body carbon and oxygen through inelastic neutron scatter [23–25], which they later combined with hydrogen and nitrogen measurement through *in vivo* NAA [26]. Until recently, most experiments utilizing fast-neutron inelastic scatter focused primarily on *in vivo* measurement of body fat.

The use of nuclear resonance scattering (NRS) was reported by Wielopolski et al. for detection of iron in the liver [27] and in the heart [28] using an indirect method of nuclear excitation by gamma rays generated through neutron capture. Recently, these authors reported the use of 14 MeV neutrons for *in vivo* measurement of liver iron through INSA and NRS [29].

In this chapter, we would discuss the development of a tomographic technique that uses inelastic scattering of fast neutrons and detection of the resulting gamma rays to quantify spatial distributions of elements in a sample. The technique, called neutron stimulated emission computed tomography (NSECT) [30, 31], was pioneered at Duke University in 2003 by the late Dr. Carey E. Floyd Jr. for the purpose of diagnostic medical imaging. NSECT uses a beam of fast neutrons to excite stable isotopes of elements in a sample to determine their concentration and spatial distribution within the sample. Since it is sensitive to a wide variety of elements that naturally occur in the human body, it has the potential to noninvasively diagnose several disorders that are characterized by changes in element concentrations in the diseased tissue [32–34].

Here we present an overview of the NSECT technique and discuss the current status of the research. The reader may note that while medical imaging of the human body is the ultimate goal of NSECT, the technique is still in development stages, with most experiments being performed on phantoms and excised tissue specimens. The methods and results presented in the chapter are mainly for the purpose of demonstrating feasibility and proof-of-concept for future medical applications.

15.1.1 Principle

The principle of NSECT can be described briefly as follows. A neutron incident on a sample travels freely along its projected path until it collides with an atomic nucleus of an element present in the sample. If the collision with the atomic nucleus results in inelastic scatter, the nucleus can get excited to one of its quantized higher-energy states. The excited nucleus is often unstable and will rapidly decay to a lower energy state, emitting a gamma-ray photon with energy equal to the difference of the two states. These energy states are well established for most elements and isotopes and are mostly unique for the elements commonly found in the body. Therefore, the energy of the emitted gamma photon can be treated as a unique signature of the emitting element. Tomographic detection and analysis of gamma lines in the emitted spectrum provide quantitative information about the spatial distribution of the element in the sample.

While the principle of NSECT is similar to that of gamma-ray emission computed tomography (G-ECT) [35], NSECT provides the advantage of being able to detect stable isotopes of elements that naturally occur in the body. Unlike G-ECT, NSECT does not require to inject radioactive tracers to the patient to produce emission decay. Stable isotopes of naturally occurring elements can be excited through inelastic scatter and detected to obtain spatial and quantitative information about their distribution in the body.

While NSECT can be used over a wide range of elements and isotopes, the elements of interest for medical applications show characteristic gamma lines with energies ranging from 350 to 6500 keV [34]. To induce gamma emission from these transitions, the energy of the incident neutrons is required to be greater than the largest energy state to be excited in the target. For most medical applications, neutron energies of approximately 7–8 MeV are sufficient to image elements found commonly in the body. NSECT applications at Duke University typically use neutron energies approximately 1 MeV greater than the highest excited state desired to compensate for energy loss in propagating through the body toward the targeted element in the tissue. For example, an investigation of ^{12}C at 4.4 MeV can be performed with a 5–6 MeV beam, whereas detection of ^{56}Fe at 847 keV can be performed with a 1.5–2 MeV beam.

As the name suggests, NSECT is a computed tomography application of neutron inelastic scatter spectroscopy. Tomography is performed using a single-beam, fixed-detector geometry similar to the acquisition mode of first-generation computed tomography systems where a single beam is translated and rotated around the object in discrete steps until the entire volume of the object is sampled [36]. In NSECT, a thin neutron beam is used to illuminate a single line through the object being scanned. Each line, also called a projection, represents the location of characteristic gamma intensities within the object. Tomography is performed by translating the object through the beam, rotating it through a fixed angle, and repeating the translation and rotation until the entire volume of the object has been scanned. The set of projections obtained

from the tomographic scan can then be reconstructed to obtain a two-dimensional image of the spatial distribution and concentration of each element in the object. It can be noted that while first-generation CT translated the beam and detector, the use of Van-de-Graaff sources in NSECT requires that the sample be moved. In both cases, the final outcome is the same (i.e., the entire volume of the sample object is scanned with the beam).

Owing to the high gamma energies observed in NSECT, it is impractical to use standard gamma cameras that are normally used in G-ECT studies. The G-ECT gamma cameras are unable to provide sufficient spatial or energy resolution for NSECT imaging. NSECT therefore uses high purity germanium (HPGe) detectors, which exhibit excellent energy resolution within the range of energies observed in body elements [37]. Unfortunately, HPGe detectors with adequate efficiency are usually large single-crystal detectors that do not have the ability to provide spatial information. Spatial information is obtained by tracking the position of the neutron beam as it illuminates a single projection path at a time through the sample. Consequently, the current implementation of NSECT requires a collimated neutron beam to facilitate tomographic acquisition.

15.1.2 Applications in Medical Imaging

NSECT has the potential for use in a variety of applications in both medical and biological imaging research. It is sensitive to a wide variety of elements that naturally occur in the human body and has the ability to provide a three-dimensional map of the elemental distribution within the target object from a single scan. These characteristics of NSECT have the potential to diagnose several disorders in the human body that are characterized by changes in element concentrations in the diseased tissue. Disorders such as iron and copper overload in the liver [38–41] and several types of cancers including breast [14, 16, 17, 42–48], prostate [49–51], and brain [52, 53] have been associated with changes in element concentrations. NSECT has the potential to diagnose these disorders through a noninvasive *in vivo* scan without the use of radioactive isotope tracers. Three potential medical and biological applications of NSECT are discussed below.

15.1.2.1 Cancer Diagnosis

Several studies have indicated that changes in trace element concentrations in human tissue may be a precursor to malignancy in several organs, such as the brain, prostate, and breast. *In vivo* measurement of such cancer-marker trace elements has the potential to differentiate between malignant and benign tissue at very early stages and enable *in vivo* cancer diagnosis through element quantification. Concentration differences measured through NAA have been reported in the breast [16, 17, 42, 45, 46, 48], colon [54–61], prostate [49, 51, 62–66], kidney [54], liver [50, 54, 67, 68], stomach [54], urinary bladder [54],

testis, and female reproductive organs [54]. NSECT cancer diagnosis can be performed by measuring the trace element composition of the tissue and analyzing this information to identify combinations of elements that are markers of cancer. Owing to NSECT's tomographic ability, given adequate sensitivity, it can identify both the location of the tumor as well as its cancer state from a single scan.

15.1.2.2 Noninvasive Measurement of Liver Iron and Copper

A second application of NSECT is in the diagnosis of liver disorders such as hemochromatosis [38–40] and Wilson's disease [41], which exhibit changes in iron and copper concentrations in the liver, respectively. Iron overload is a serious concern for patients with thalassemia, sickle cell anemia, and hemochromatosis mutations and for other patients who receive chronic blood transfusions. Similarly, copper overload is observed in patients with Wilson's disease. The current definitive diagnostic technique for these disorders is invasive liver biopsy followed by chemical analysis of iron to determine the severity of the disorder [38, 40, 69]. NSECT provides a noninvasive alternative with the potential to obtain the same information without the need for a biopsy. Several different techniques (reported in [33]) have attempted to detect and quantify iron concentration in the liver *in vivo*, for example, X-ray computed tomography (X-ray CT), MRI, magnetic resonance spectroscopy (MRS), super-conducting quantum interference susceptometry (SQUID), and nuclear resonance scattering (NRS) [27, 70–88]. While each has had varying degrees of success, few have found widespread acceptance in the clinical environment. Both X-ray CT and MRI lack the sensitivity required for detecting mild to moderate degrees of iron overload, and MRI also shows reduced sensitivity in cases of severe iron overload [75, 76, 80, 89]. In MRS, the low signal from bound iron makes quantification studies difficult. MRS also has limited resolution (larger than 1 cm) [90]. While SQUID has found some success in detecting liver iron, there are only about four SQUID facilities in the world that offer iron overload testing, making it difficult to translate into a widely used clinical alternative. NRS has achieved some success in patients with iron overload but with high levels of dose [27]. NSECT has the potential to overcome many of these limitations and develop into a clinical technique for noninvasive measurement of liver iron and copper [33].

15.1.2.3 Small Animal Imaging

A third potential area of application for NSECT is in the spectroscopic imaging of small animals [91, 92] to understand the structural and functional mechanisms of metabolism and transport of elements in normal and disease models. For example, NSECT can be used to follow the metabolic migration of nutrients in normal and in genetically modified mice, measurement of iron and calcium levels in the cardiac wall, and molecular transport and drug delivery studies where molecules of interest are tagged with stable isotopes rather than radioactive tracers.

NSECT represents a technique that combines both anatomic and functional imaging. Through CT acquisition, it is possible to obtain a three-dimensional map of element distribution within a specific organ, thereby providing anatomic information about the location and extent of the diseased tissue. Simultaneously, information about elements within the tissue can provide information about the functional (disease) state of the tissue.

15.2 Imaging Facility and Apparatus

All NSECT experiments performed so far have been conducted at the Triangle Universities Nuclear Laboratory (TUNL) accelerator facility located at Duke University. TUNL is a low energy nuclear physics research laboratory with a 10 MeV tandem Van-de-Graaff accelerator capable of producing 20 MeV proton or deuteron beams and a host of other light ion beams. The shielded neutron source provides researchers with an intense pulsed collimated mono-energetic neutron beam with energies between 5 and 23.2 MeV. A detailed description of the facilities and apparatus used in NSECT has been provided in [32, 34].

Three key components are required in an NSECT acquisition system: (a) neutron source, (b) gamma detector, and (c) tomographic acquisition and reconstruction technique. Each of these components is readily available at TUNL. Figure 15.1 shows a schematic of an NSECT system with the major components. A description of the key components is given below.

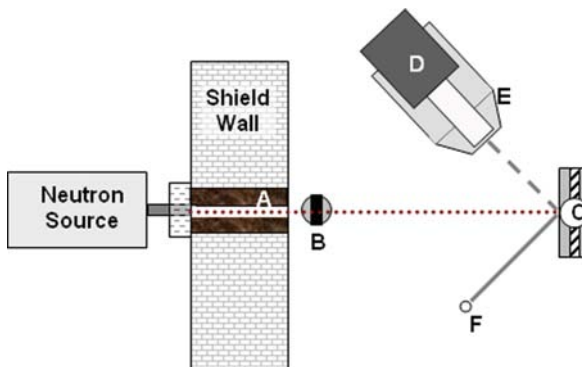


Fig. 15.1 Schematic of an NSECT system used in tomographic measurements. Major components of the system are labeled as A – Neutron Collimator; B – Instantaneous Neutron Flux Monitor; C – Sample Manipulation Tomographic Gantry; D – HPGe detector; E – Anticoincidence Compton Shield; and F – Inelastically Scattered Neutron. The neutron beam (shown by the line of dots) travels from the source to the sample (C) and scatters inelastically. Gammas emitted in the inelastic scatter interaction (shown as line of dashes) are detected by the HPGe detector, while the scattered neutron (F) continues along another trajectory (shown as a solid line). (Figure modified from [94] pp. 2313–2326. © Institute of Physics and IOP Publishing Limited 2008)

15.2.1 Neutron Source

NSECT can be performed with a variety of neutron sources, some of which are available commercially, while others are specialized sources available only at state-of-the-art neutron facilities. An ideal source for an NSECT application should produce a narrow collimated beam of fast neutrons with high neutron flux and allow beam pulsing and energy tuning with a nearly monochromatic energy profile. High neutron flux is required to achieve minimal scan durations, while a collimated beam is required to attain spatial resolution in the tomographic acquisition. Beam pulsing or chopping is necessary to identify the time-resolved inelastic scatter signal and separate it from other neutron and gamma effects that occur later in time. Without beam pulsing (i.e., with a continuous-beam source), the inelastic scatter signal can be obscured by radiation detected from room and sample-related background effects that are observed at different times, such as radioactive decay following neutron capture in the sample. These effects can be reduced through time-of-flight (TOF) correction, which needs beam pulsing. The TOF correction technique for NSECT has been described in detail in a separate publication [93].

Energy tuning, while highly desirable, is not an essential requirement for a neutron source. A requirement of inelastic scatter spectroscopy is that the energy of the neutron beam must be higher than the maximum energy state to be excited. However, unnecessarily high neutron energies will simply excite higher unwanted states in both desired and undesired elements, leading to a busy spectrum cluttered with noise. Further, as NSECT detectors are susceptible to Compton noise from high gamma energies, exciting unwanted high energy states in the sample will also produce higher Compton background noise signals in the detectors, which can potentially obscure elements with low-lying characteristic gamma lines. A monochromatic energy source producing neutrons with energy slightly higher than the highest desired excited state is the most suitable. With a tunable neutron source, a beam can be produced with energy that is sufficient to excite the elements of interest and avoid other unwanted elements in the sample. For example, to image carbon in a biological sample (at 4.439 MeV), a neutron energy of 5.0 – 5.5 MeV is ideal as it excites the 4.439 MeV energy state in ^{12}C but avoids excitation of the 6.13 MeV excited state in ^{16}O . A monochromatic source also facilitates lower patient dose by restricting neutron illumination to the required range of energy. Higher neutron energies that contribute to dose by depositing more energy per interaction and lower thermal energies that contribute to dose through neutron capture and subsequent radioactive emission are eliminated in a true monochromatic source.

Table 15.1 lists some neutron sources that have been identified for use in NSECT: Van-de-Graaff accelerators, deuterium-deuterium (DD) neutron tubes, and deuterium-tritium (DT) neutron tubes. Van-de-Graaff accelerators provide tunable collimated neutron beams that are suitable for tomography. NSECT experiments performed thus far have used a Van-de-Graaff accelerator

Table 15.1 A comparison of three neutron sources suitable for NSECT applications

Characteristic	Van-de-Graaff	DD Neutron Tube	DT Neutron Tube
Energy	5 MeV to 23.2 MeV	3.2 MeV	14 MeV
Flux	$10^4 - 10^6$ n/s.cm ²	$10^8 - 10^{11}$ n/s	$10^{10} - 10^{13}$ n/s
Pulsing	2 ns @ 2.5 MHz	100 μ s	100 μ s
Collimation	Available	Available	Available
Monochromatic Beam	Yes	Yes	Yes
Energy Tuning	Yes	No	No

at Duke University as the source of neutrons. The accelerator produces a tunable, monochromatic, pulsed neutron beam, which can be tuned to energies between 5 and 23.2 MeV and produces collimated fluxes of 10^4 – 10^6 n/s.cm². The beam can be collimated to any desired shape and size using collimator inserts and is pulsed to provide 2 ns wide bunches at the target to allow measurement of neutron and gamma TOF. The repetition rate of the beam pulses is adjustable from 2.5 MHz down to 39 kHz [32]. Beams measuring 0.8 cm at full width at half maximum have been used to obtain image resolution of approximately 1 cm [94].

DD and DT neutron tubes produce high-flux monochromatic beams and possess the advantage of being commercially available. DD tubes produce neutrons at 3.2 MeV, while DT tubes produce neutrons at 14.2 MeV. Owing to the required neutron energy constraint, DD tubes are not suitable for applications that require the imaging of carbon or oxygen. Both tubes can be pulsed down to 100 μ s or operated in continuous mode, and collimation is available at the cost of neutron flux.

A thin neutron plastic scintillator attached to a photomultiplier tube acts as an instantaneous neutron flux monitor to measure fluctuations in the neutron beam current. The attenuation of neutrons by the flux monitor in the energy range of current NSECT studies is typically less than 0.1%.

15.2.2 Gamma Detector

As mentioned earlier, most elements of interest for medical NSECT applications show characteristic gamma lines with energies ranging from 350 to 6500 keV. In some elements, gamma lines differ by as little as 4 keV (e.g., ²⁷Al at 843.7 keV and ⁵⁶Fe at 846.7 keV). NSECT gamma detectors must therefore possess excellent energy resolution as well as high efficiency at high gamma energies. Standard gamma camera detectors used in nuclear medicine studies are unable to provide the energy resolution and efficiency required and, therefore, cannot be used for NSECT applications.

Several gamma-ray detectors have been explored and evaluated for use in NSECT, including single-crystal and clover HPGe detectors and the comparatively inexpensive options NaI-Tl and BGO. For multielement applications, such as cancer diagnosis, only HPGe detectors are found to be suitable, providing the most desirable combination of energy resolution and efficiency. HPGe detectors typically possess energy resolution of 0.1%, providing approximately 1 keV resolution at 1 MeV. BGO and NaI-Tl detectors provide typical energy resolutions of approximately 7 and 12%, respectively, which is insufficient to separate close-lying gamma lines in a multielement analysis. However, these detectors are suitable for single-element evaluations where the element of interest lies in a region, which is free from close-lying gamma lines from other elements.

NSECT experiments performed at Duke University have used two HPGe segmented detectors in the two fold segmented clover detector configuration. In this configuration, each detector consists of four coaxial n-type germanium crystals mounted together in the shape of a 4-leaf clover. Each detector exhibits minimum relative efficiency of 22% (relative efficiency compares the efficiency of the detector at 1332 keV to that of a 3 inch cubic NaI detector) and full width at half maximum less than or equal to 2.25 keV for 1.332 MeV gamma rays of ^{60}Co . Detectors are typically calibrated against a ^{22}Na source and positioned at ± 135 degrees from the incident neutron beam. A majority of the elements of interest to NSECT decay through electric quadrupole transitions, whose distribution has maximum intensity at 45 and 135 degrees. Placing the detectors at the 135 degree orientation helps to maximize signal intensity and simultaneously prevent detector activation and damage from forward scattering neutrons. In Figure 15.1, the HPGe detector (labeled D) is visible surrounded by an anticoincidence Compton shield (labeled E), which is used to reduce the effects of Compton scattering in the detectors. These shields have a minimum peak-to-Compton ratio of 41 for ^{60}Co gamma rays at 1.332 MeV [32].

15.2.3 Tomographic Acquisition Gantry

As with all other tomographic imaging systems, NSECT performs tomography by acquiring a complete set of projections of line integrals through the sample. For NSECT, these projections are defined by the angular and spatial sampling intervals between successive positions of the beam on the sample. Acquisition is performed in a manner similar to first generation CT with a stationary beam and single element detector located at fixed positions with respect to each other. The sample is translated through the beam, rotated through a finite angle, and translated through the beam again. The process is repeated until the volume of interest in the sample has been scanned. While ideal tomography systems would acquire projections between 0 and 360 degrees, due to limitations in acquisition time and concerns about patient dose, the current NSECT tomography system scans the sample from 0 to 180 degrees and employs the maximum likelihood expectation maximization (MLEM) technique [95] for reconstruction. The

MLEM technique is able to take into account parameters such as nonuniform and partial sampling when reconstructing an image.

Tomography is performed using the single-beam, fixed-detector geometry of first-generation computed tomography systems where a thin neutron beam is used to illuminate a single line (projection) through the object being scanned. Tomography is performed by translating the object through the beam, rotating it through a fixed angle, and repeating the translation and rotation until the entire volume of the object has been scanned. The set of projections obtained from the tomographic scan are then reconstructed to obtain a two-dimensional image of the spatial distribution and concentration of each element in the object.

Figure 15.1 shows the tomographic computer-controlled gantry (labeled C), which enables tomographic acquisition by translating and rotating the sample with respect to the neutron beam.

Reconstruction can be performed through any available reconstruction algorithm. While a variety of algorithms are available, the MLEM algorithm is selected due to its superiority of performance in undersampled acquisition systems and its ability to incorporate the Poisson nature of photon counting [95], both characteristics important to NSECT. An analysis of the MLEM algorithm and its advantages over other iterative and Fourier techniques for image reconstruction in NSECT has been described in [96].

Data acquisition can be performed using any nuclear spectroscopy acquisition system that allows acquisition and storage of raw data and offline retrieval for data visualization and analysis. Examples of such software that has been used at Duke include CODA [97] and SpecTel [98].

15.3 Current Applications

There are many diverse and exciting applications where NSECT can potentially be used to make a clinical diagnosis through noninvasive tomography. Disorders, such as cancer, hemochromatosis (liver iron overload), and Wilson's disease (liver copper overload), can be diagnosed by identifying the concentrations of the respective disease-marking elements in the tissue or organ. Several experiments have been performed to investigate the feasibility of diagnosing these disorders through NSECT, using both tomographic acquisition as well as nontomographic (single projection) spectroscopy. The results of some of these experiments are described below.

15.3.1 Experiment 1: Tomographic Acquisition of Multielement Phantom

Figure 15.2 shows an image of a solid iron-copper phantom containing bars of natural iron and natural copper arranged in the shape of the letter 'N.' Each bar



Fig. 15.2 Geometry of the phantom imaged in the tomography experiment. The vertical outer bars represent copper while the diagonal inner (gray) bars represent iron. Each bar measures 0.6 cm by 6 cm by 2.5 cm.

(Figure from Floyd et al, "Neutron Stimulated Emission Computed Tomography of a Multi-Element Phantom," *Phys Med Biol*, vol. 53, pp. 2313–2326. © Institute of Physics and IOP Publishing Limited 2008)

measures 6 mm in width, 60 mm in height, and 25 mm in depth. The phantom was scanned with an 8 mm wide 7.5 MeV neutron beam with 11 spatial projection at 8 angles. As can be seen in Fig. 15.3, the corresponding NSECT reconstructed image shows excellent agreement with the spatial locations of iron and copper within the image. Images were reconstructed individually for each of the two elements and then combined to generate the figure shown. Reconstructed resolution was observed to be approximately 1 cm, which is reasonable for a beam that measured 8 mm at full width at half maximum. The experiment demonstrates the tomographic ability of NSECT in identifying spatially individual elements in a multielement sample.

Figure 15.4 shows the corresponding gamma spectrum from the NSECT scan of the iron-copper phantom. Six spectral lines can be identified for energy transitions from iron and copper in the phantom.

Detailed analysis and a complete description of the experiment are available in [94].

15.3.2 Experiment 2: Diagnosis of Iron Overload in Human Liver Phantom

Figure 15.5 shows a human torso phantom with two chambers – an outer chamber corresponding to an adult torso and an inner chamber corresponding

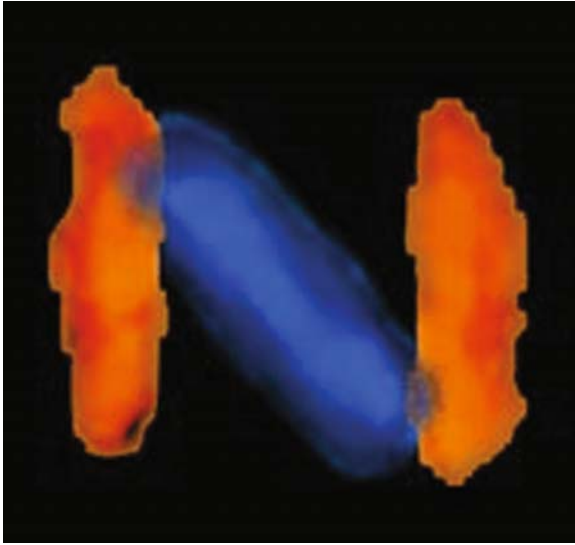


Fig. 15.3 Reconstructed image from the NSECT acquisition of the sample. The vertical outer regions represent copper while the diagonal inner region represents iron. Each element was reconstructed separately and then combined.

(Figure from Floyd et al, "Neutron Stimulated Emission Computed Tomography of a Multi-Element Phantom," *Phys Med Biol*, vol. 53, pp. 2313–2326. © Institute of Physics and IOP Publishing Limited 2008)

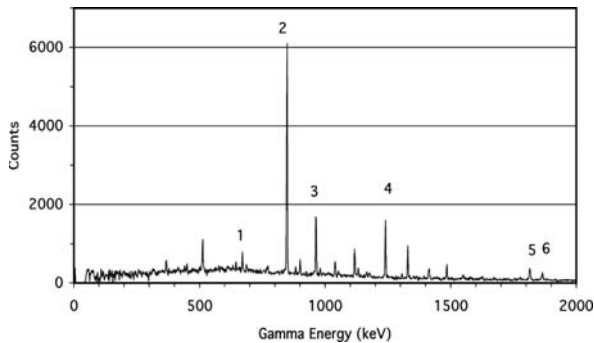


Fig. 15.4 Gamma energy spectrum from the iron-copper phantom showing spectral lines from six transitions in ^{56}Fe and ^{63}Cu :

1. ^{63}Cu from 1st excited state to ground state; energy 660 keV
2. ^{56}Fe from 1st excited state to ground state; energy 847 keV
3. ^{63}Cu from 2nd excited state to ground state; energy 962 keV
4. ^{56}Fe from 3rd to 2nd excited state; energy 1239 keV
5. ^{56}Fe from 4th to 2nd excited state; energy 1811 keV
6. ^{63}Cu from 6th to 1st excited state; energy 1864 keV

(Figure from [94] pp. 2313–2326. © Institute of Physics and IOP Publishing Limited 2008)



Fig. 15.5 A phantom of the human torso with two chambers – outer chamber corresponding to an adult torso, and inner chamber corresponding to an adult human liver. Both chambers can be filled separately with any desired material.
(Figure from Kapadia et al. [32], pp. 2633–2649. © Institute of Physics and IOP Publishing Limited 2008)

to an adult human liver. The phantom was filled with bovine liver tissue with artificially induced iron overload and was scanned using a 5 MeV neutron beam. The resultant spectrum shown in Fig. 15.6 was analyzed to quantify the concentration of iron in the liver. The gamma line at 847 keV was detected for 4.18 g of ^{56}Fe . Based on this spectrum, a clinically relevant projected sensitivity of 6 mg/g was obtained for iron overload diagnosis. In addition, gamma lines were identified for several other elements in the liver, including Cl, Cu, K, Na, and Zn, which were confirmed through NAA, and for ^{12}C from the phantom. Gamma lines were also identified for ^{74}Ge and ^{76}Ge from the gamma-ray detectors, ^{42}K from the room background, and ^1H (neutron capture) from the phantom. The dose from the scan was calculated using a Monte-Carlo simulation as 0.375 mSv [33], which is significantly lower than an abdominal X-ray exam that typically delivers 2 mSv [99]. The experiment demonstrates that NSECT has the potential to detect clinically relevant concentrations of iron in the human body through a noninvasive scan with reasonable dose. Although the scan time for this experiment was unreasonable at over 24 h, it

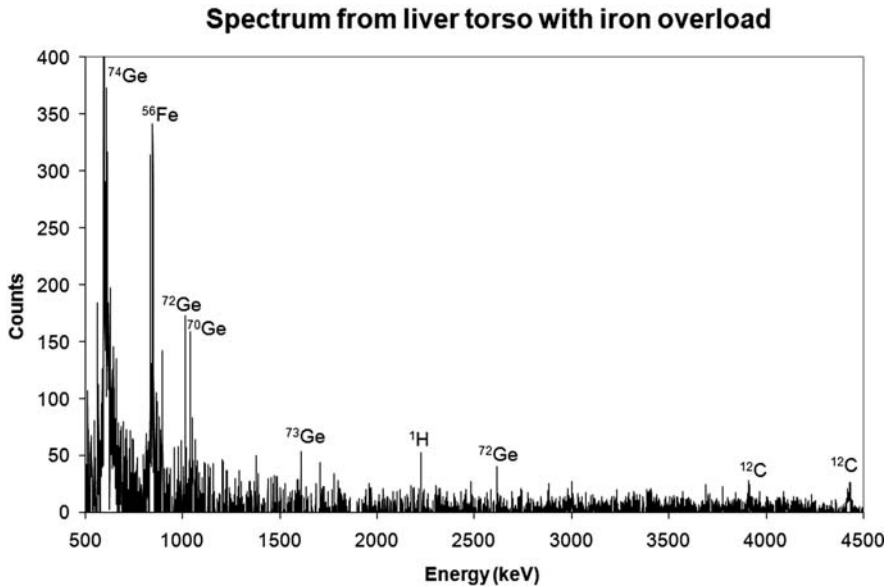


Fig. 15.6 Gamma energy spectrum from the uniform iron overload torso phantom, showing peaks corresponding to elements detected in the liver. The peak at 847 keV corresponds to ^{56}Fe . Peaks are also seen for Ge from the detector and ^{12}C and ^1H from the tissue. (Figure from Kapadia et al. [32], pp. 2633–2649. © Institute of Physics and IOP Publishing Limited 2008)

can be brought down to a few seconds using high-flux neutron sources (such as the aforementioned DD and DT tubes) and increasing the number of detectors.

Detailed analysis and a complete description of the experiment are available in [33].

15.3.3 Experiment 3: Detection of Breast Cancer

To investigate the feasibility of breast cancer detection through NSECT (Figs. 15.7 and 15.8), samples of benign and malignant breast tissue obtained through breast biopsy were scanned with a 6 MeV neutron beam for a cumulative dose of 1 mSv each. After TOF and sample-out background subtraction, the resultant spectra were analyzed to identify elements that showed statistically significant differences between the two samples. Concentration differences were found for Al, Br, Cl, Co, Fe, K, Rb, and Zn, of which Cl, Fe, K, and Zn were verified through NAA. The experiment demonstrates that NSECT can potentially be used to detect several cancer-marking elements in human tissue.

Table 15.2 gives a list of elements that showed statistically significant differences between the benign and malignant spectra. While several elements were identified with concentration differences in each of the two samples, NAA analysis of the samples determined that their concentration was of the order

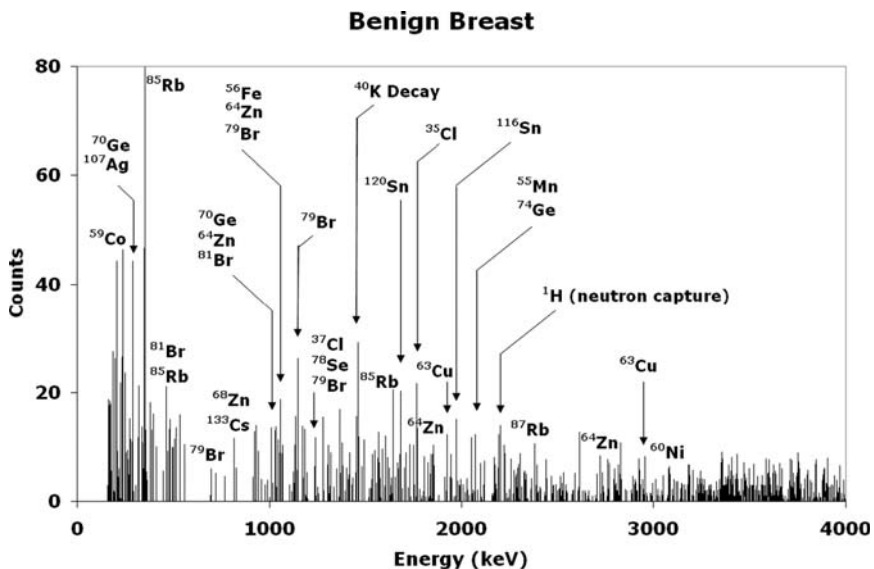


Fig. 15.7 NSECT spectrum of a benign breast sample showing elements identified through NSECT spectroscopy. (Figure from Kapadia et al. [32], pp. 501–509. © 2008 IEEE)

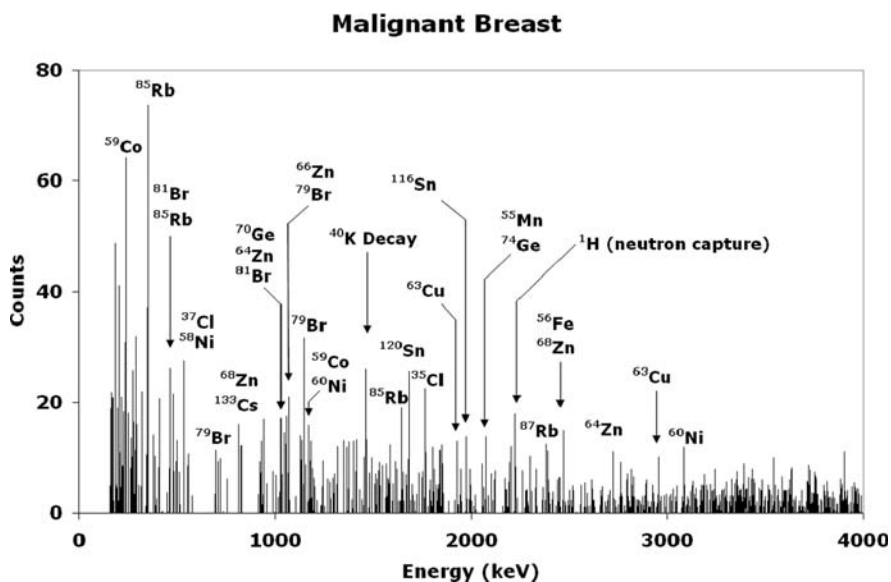


Fig. 15.8 NSECT spectrum of a malignant breast sample showing elements identified through NSECT spectroscopy. (Figure from Kapadia et al. [32], pp. 501–509. © 2008 IEEE)

Table 15.2 List of elements showing statistically significant differences between benign and malignant spectra. Elements with negative differences showed a decrease in concentration in the malignant sample. Statistical significance was calculated using a z-score test for difference of means. (Table from Kapadia et al. [32], pp. 501–509. © 2008 IEEE)

Energy keV	Element match	Counts benign	Counts malignant	Diff	p-val
219	⁷⁹ Br	6	19	13	0.01
397	⁵⁹ Co, ⁷⁹ Br	16	2	-14	0.01
1028	⁸¹ Br	13	29	16	0.05
1128	³⁹ K, ⁶⁸ Zn	0	13	13	0.001
1306	⁵⁶ Fe	10	0	-10	0.01
2299	²⁷ Al	0	13	13	0.001
2469	³⁷ Cl, ⁵⁶ Fe, ⁶⁶ Zn	5	15	10	0.05
3635	³⁵ Cl	3	14	11	0.01

of a few hundred micrograms, which is below the sensitivity of the current system, which is a few hundred milligrams [32]. Therefore, accurate quantification of these microgram concentrations will require a significant improvement in sensitivity.

Detailed analysis and a complete description of the experiment are available in [32].

15.4 Dose Analysis

Patient dose in NSECT is of significant concern due to the use of fast neutrons, which have a dose quality factor (Q-factor) of 10. For the technique to translate successfully to the clinical environment, NSECT dose must be comparable to the dose levels of other ionizing imaging modalities. As the technique is still in early stages of development, dose analysis in NSECT is currently performed using Monte-Carlo simulations. The process, described in [96, 100], can be summarized in the following three steps:

- (a) a Monte-Carlo simulation is used to estimate two parameters for an incident neutron beam – the number of neutrons that interact in the volume of interest and the average energy deposited per interacting neutron,
- (b) the resulting energy deposited in the volume is converted from MeV to J/kg using the known mass of the volume to give the absorbed energy in Gray (Gy), and
- (c) the absorbed energy is multiplied by the quality factor for neutrons (10) and the weighting factor for the organ of interest to give the effective dose equivalent in Sieverts (Sv).

This technique has been used to calculate the patient dose for NSECT scans of the abdomen [96], liver [33, 96, 100], and breast [100, 101]. Table 15.3 summarizes the results of these dose-analysis simulations.

In comparison, an abdominal X-ray scan typically delivers 2 mSv, a mammogram delivers 0.7 mSv, while an abdominal CT exam delivers approximately 10 mSv [99]. The doses from NSECT scans appear comparable to, or even lower than, the other techniques. This is largely due to the modest number of neutrons

Table 15.3 NSECT dose delivered to organs in the body from NSECT scans

Organ	Spectroscopic scan	Tomography scan
Abdomen	1–2 mSv	1–5 mSv
Liver	0.02–1 mSv	0.5–3 mSv
Breast	0.02–0.5 mSv	0.5–1 mSv

required to create an NSECT image or extract sufficient information from the sample. Preliminary simulation studies indicate that as few as 10 million incident neutrons are required to obtain quantitative accuracy of 95% in a tomographic image [102]. A fluence of 10 million incident neutrons on the breast, for example, corresponds to a dose of less than 1 mSv. Dose levels in NSECT can potentially be reduced even further by increasing the number of gamma-ray detectors and using high-flux neutron sources to reduce scan time.

15.5 Summary

NSECT represents an exciting new imaging modality that has the potential for application in both medical and biological research. Several human disorders characterized by element changes can be diagnosed through noninvasive *in vivo* scanning using this technique. NSECT has the ability to obtain tomographic information about the spatial distribution of elements within a tissue or organ to make a quantitative and spatial diagnosis. A prototype of the NSECT acquisition system has been developed and built at Duke University using a Van-de-Graaff accelerator and HPGe detectors. As demonstrated through experiments with the prototype system, NSECT has the sensitivity to detect concentrations of iron that represent a clinically relevant liver iron overload condition. Sensitivity evaluation experiments indicate that concentrations as low as 3 mg/g may be quantifiable through NSECT. Although MRI is able to quantify moderate concentrations of iron overload, it suffers from a loss of accuracy for concentrations above 6 mg/g wet weight (20 mg/g dry weight) due to a reduction in the signal intensity caused by high concentrations of iron [89]. NSECT, on the other hand, shows an increase in the signal with increasing iron concentration. This facilitates iron overload detection in patients with severe overload, where MRI begins to lose accuracy.

The image resolution observed with the prototype system is approximately 1 cm, which is passable for imaging large organs such as the liver. However, as the resolution depends primarily on the width of the neutron beam, it is possible to improve the resolution significantly by using a narrow collimated beam (at the cost of additional scan time). Simulation experiments have demonstrated a resolution of 5 mm when scanning was performed with a 5 mm rectangular beam [96]. While the resolution of the NSECT system depends primarily on the size of the incident neutron beam, the best resolution achievable in a hydrogen-rich biological sample will also be limited by the noise component generated from neutron scatter by hydrogen. Neutrons that are meant to illuminate a certain voxel in the sample may

scatter onto adjacent voxels containing an element of interest and induce inelastic gamma emission from that voxel. Detection of the adjacent-voxel gammas may lead to a spread in the tails of the resulting sinograms, which can lead to reduced resolution. The contribution of this effect to the limits of resolution is currently being investigated through Monte-Carlo simulations.

Patient dose for NSECT examinations of different organs have been found to vary between 0.02 mSv for a breast spectroscopic exam [101] to under 1 mSv [96] for a liver spectroscopic exam, evaluated through Monte-Carlo simulations. Tomographic doses are slightly higher depending on the number of projections used but are generally lower than the dose delivered from a corresponding X-ray CT exam [96].

15.6 Future

The current focus of NSECT has been on quantitative diagnosis of large-organ disorders (e.g., those of the liver), largely due to the limits of resolution and sensitivity observed in the prototype system. As these limiting effects are understood better, efforts to improve the sensitivity and resolution of the system are being made. Improved sensitivity will facilitate the diagnosis of a greater number of disorders, including several types of cancer. The use of portable neutron sources such as pulsed DD and DT tubes is being explored to develop a portable, high-flux scanning solution for use in a clinical environment. Such portable tomographic scanning systems with improved resolution and sensitivity will present an attractive method for human and small-animal imaging and for diagnosis and screening of several disorders in the human body.

Acknowledgment The author would like to acknowledge and thank all the members of the Duke Advanced Imaging Laboratories (DAILabs) and Triangle Universities Nuclear Laboratory (TUNL) who have been involved in the development of NSECT, especially Georgia Tourassi, Amy Sharma, and Janelle Bender for their analytical contribution and deep involvement in NSECT; Brian Harrawood for his unparalleled computing support; Calvin Howell, Alexander Crowell, Matthew Kiser, and Robert Macri for their help and guidance with NSECT acquisition experiments; and Anton Tonchev and Anthony Hutcheson for their help with gamma detector setup and management. Finally, the author would like to express his deep gratitude to Dr. Carey Floyd, the pioneer of NSECT, in whose memory and name this research continues.

References

1. J. Anderson, S.B. Osborn, R.W. Tomlinson, D. Newton, J. Rundo, L. Salmon, and J.W. Smith, Neutron-Activation Analysis in Man in Vivo. a New Technique in Medical Investigation, *Lancet* **2**, 1201–1205, (Dec 5 1964).
2. M.J. Chamberlain, J.H. Fremlin, D.K. Peters, and H. Philip, Total body sodium by whole body neutron activation in the living subject: further evidence for non-exchangeable sodium pool, *Br. Med. J.* **2**, 583–585 (Jun 8, 1968).

3. M.J. Chamberlain, J.H. Fremlin, D.K. Peters, and H. Philip, Total body calcium by whole body neutron activation: new technique for study of bone disease, *Br. Med. J.* **2**, 581–3, Jun 8 1968.
4. M.J. Chamberlain, J.H. Fremlin, D.K. Peters, and H. Philip, Measurement of whole body calcium and sodium by neutron activation analysis in the living subject, *Strahlentherapie [Sonderb.]*, **67**, 178–85, 1968.
5. M.J. Chamberlain, Whole-body neutron activation analysis, *Proc. R. Soc. Med.* **62**, 370–3 (Apr 1969).
6. M.J. Chamberlain, J.H. Fremlin, I. Holloway, and D.K. Peters, Use of the cyclotron for whole body neutron activation analysis: theoretical and practical considerations, *Int. J. Appl. Radiat. Isot.* **21**, 725–34 (Dec 1970).
7. M.J. Chamberlain, J.H. Fremlin, D.K. Peters, and H. Philip, Applications of the whole-body counter in total-body neutron activation analysis, *Br. J. Radiol.* **43**, 287–8 (Apr 1970).
8. M.J. Chamberlain and J.H. Fremlin, Measurement of whole-body nitrogen by pulsed neutron activation analysis, *Strahlentherapie [Sonderb.]* **72**, 88–93 (1972).
9. S.H. Cohn and C.S. Dombrowski, Measurement of total-body calcium, sodium, chlorine, nitrogen, and phosphorus in man by in vivo neutron activation analysis, *J. Nucl. Med.* **12**, 499–505 (Jul 1971).
10. D. Vartsky, K.J. Ellis, and S.H. Cohn, In vivo measurement of body nitrogen by analysis of prompt gammas from neutron capture, *J. Nucl. Med.* **20**, 1158–1155 (Nov 1979).
11. C.L. Hollas, L.E. Ussery, K.B. Butterfield, and R.E. Morgado, A method for in vivo determination of carbon and oxygen using prompt gamma radiations induced by 14.7-MeV neutrons, *Basic Life Sci.* **55**, 395–400 (1990).
12. H.C. Biggin, N.S. Chen, K.V. Ettinger, J.H. Fremlin, W.D. Morgan, R. Nowotny, M.J. Chamberlain, and T.C. Harvey, Cadmium by in vivo neutron activation analysis, in *J. Radioanal. Chem.*, v. 19, no. 2, pp. 207–214; *International colloquium on activation analysis of very low amounts of elements; 2 Oct 1972; Saclay, France* United Kingdom (1974).
13. M.L. Arnold, F.E. McNeill, I.M. Stronach, A. Pejovic-Milic, D.R. Chettle, and A. Waker, An accelerator based system for in vivo neutron activation analysis measurements of manganese in human hand bones, *Med. Phys.* **29**, 2718–24 (Nov 2002).
14. A. Garg, V. Singh, et al., An elemental correlation study in cancerous and normal breast tissue with successive clinical stages by neutron activation analysis, *Biol. Trace Element Res.* **46**, 185–202 (1994).
15. A. Danielsen and E. Steinnes, A study of some selected trace elements in normal and cancerous tissue by neutron activation analysis, *J. Nucl. Med.* **11**, 260–4 (Jun 1970).
16. K.H. Ng, D.A. Bradley, and L.M. Looi, Elevated trace element concentrations in malignant breast tissues, *Br. J. Radiol.* **70**, 375–82 (Apr 1997).
17. K.H. Ng, D.A. Bradley, L.M. Looi, C.S. Mahmood, and A.K. Wood, Differentiation of elemental composition of normal and malignant breast tissue by instrumental neutron activation analysis, *Appl. Radiat. Isot.* **44**, 511–6 (Mar 1993).
18. K.J. Ellis, Human body composition: in vivo methods, *Physiol. Rev.* **80**, 649–80 (Apr 2000).
19. J.F. Sutcliffe, A review of in vivo experimental methods to determine the composition of the human body, *Phys. Med. Biol.* **41**, 791–833 (May 1996).
20. E. Witkowska, K. Szczepaniak, and M. Biziuk, Some applications of neutron activation analysis: A review, *J. Radioanal. Nucl. Chem.* **265**, 141–150 (2005).
21. S. Mattsson and B.J. Thomas, Development of methods for body composition studies, *Phys. Med. Biol.* **51**, R203–28 (Jul 7 2006).
22. K. Kyere, B. Oldroyd, C.B. Oxby, L. Burkinshaw, R.E. Ellis, and G.L. Hill, The feasibility of measuring total body carbon by counting neutron inelastic scatter gamma rays, *Phys. Med. Biol.* **27**, 805–17 (Jun 1982).

23. J.J. Kehayias, S.B. Heymsfield, A.F. LoMonte, J. Wang, and R.N. Pierson, Jr., In vivo determination of body fat by measuring total body carbon, *Am. J. Clin. Nutr.* **53**, 1339–44 (Jun 1991).
24. J.J. Kehayias, Aging and body composition: possibilities for future studies, *J. Nutr.* **123**, 454–8 (Feb 1993).
25. J.J. Kehayias, H. Zhuang, V. Hughes, and L. Dowling, Assessment of body fat and lean in the elderly by measuring body carbon and oxygen: validation against hydrodensitometry, *Appl. Radiat. Isot.* **49**, 723–5 (May-Jun 1998).
26. J.J. Kehayias, S. Valtuena, A.B. Waitekus, C.A. Sheahan, and M. O'Neill, In vivo elemental partition analysis using fast neutrons. A tool for testing the efficacy of new clinical interventions, *Ann. N Y. Acad. Sci.* **904**, 140–7 (May 2000).
27. L. Wielopolski, R.C. Ancona, R.T. Mossey, A.N. Vaswani, and S.H. Cohn, Nuclear resonance scattering measurement of human iron stores, *Med. Phys.* **12**, 401–4 (Jul-Aug 1985).
28. L. Wielopolski and E.C. Zaino, Noninvasive in-vivo measurement of hepatic and cardiac iron, *J. Nucl. Med.* **33**, 1278–82 (Jul 1992).
29. L. Wielopolski, Feasibility of measuring iron in vivo using fast 14 MeV neutrons, *Cooley's Anemia Foundation Inc. BNL-7980–2005* (2005).
30. C.E. Floyd, C.R. Howell, B.P. Harrawood, A.S. Crowell, A.J. Kapadia, R. Macri, J.Q. Xia, R. Pedroni, J. Bowsher, M.R. Kiser, G.D. Tourassi, W. Tornow, and R. Walter, Neutron Stimulated Emission Computed Tomography of Stable Isotopes, in *SPIE Symposium on Medical Imaging*, San Diego, CA, pp. 248–254 (2004).
31. C.E. Floyd, J.E. Bender, A. Sharma, A. Kapadia, J. Xia, B. Harrawood, G.D. Tourassi, J. Lo, and C.R. Howell, Introduction to Neutron Stimulated Emission Computed Tomography. *Phys. Med. Biol.* **50** (14), 3375–90 (2005).
32. A.J. Kapadia, A.C. Sharma, J.E. Bender, G.D. Tourassi, C.R. Howell, A.S. Crowell, M.R. Kiser, B.P. Harrawood, and C.E. Floyd, Neutron Stimulated Emission Computed Tomography for Diagnosis of Breast Cancer, *IEEE Trans Nucl. Sci.* **55**, 501–509 (2008).
33. A.J. Kapadia, G.D. Tourassi, A.C. Sharma, A.S. Crowell, M.R. Kiser, and C.R. Howell, Experimental detection of iron overload in liver through neutron stimulated emission spectroscopy, *Phys. Med. Biol.* **53**, 2633–2649 (2008).
34. C.E. Floyd, J.E. Bender, A.C. Sharma, A.J. Kapadia, J.Q. Xia, B.P. Harrawood, G.D. Tourassi, J.Y. Lo, A.S. Crowell, and C.R. Howell, Introduction to neutron stimulated emission computed tomography, *Phys. Med. Biol.* **51**, 3375–3390 (2006).
35. M.N. Wernick and J.N. Aarsvold, *Emission Tomography: The Fundamentals of PET and SPECT*: Academic Press, San Diego (2004).
36. A. Kak and M. Slaney, *Principles of computerized tomographic imaging* vol. 33. Philadelphia: society for industrial and applied mathematics (2001).
37. J.E. Bender, C.E. Floyd, B.P. Harrawood, A.J. Kapadia, A.C. Sharma, and J.L. Jesneck, The effect of detector resolution for quantitative analysis of neutron stimulated emission computed tomography, in *SPIE Medical Imaging*, pp. 1597–1605 (2006).
38. L.W. Powell, Diagnosis of hemochromatosis, *Semin. Gastrointest Dis.* **13**, 80–8 (Apr 2002).
39. S. Joffe, Hemochromatosis, N. Lamki, B. Coombs, U. Schmiedl, R.M. Krasny, and J. Karani, Eds., *Medscape emedicine*, emedicine.medscape.com/article/369012-overview, Mar 11, 2005.
40. L. Powell, Hemochromatosis, in D. Kasper, Fawci, AS, Longo, DL, Braunwald, E, Hauser, SL, Jameson, JL, Ed., *Harrison's Principles of Internal Medicine*, 16 ed. vol. 2, McGraw Hill, New York, NY, pp. 2298–2303 (2005).
41. G. Brewer, Wilson Disease, in D. Kasper, Fawci, AS, Longo, DL, Braunwald, E, Hauser, SL, Jameson, JL, Ed., *Harrison's Principles of Internal Medicine*, 16 ed. vol. 2, NY: McGraw Hill, pp. 2313–2315 (2005).
42. H. Mussalo-Rauhamaa, S. Piepponen, J. Lehto, R. Kauppila, and O. Auvinen, Cu, Zn, Se and Mg concentrations in breast fat of Finnish breast cancer patients and healthy controls, *Trace Elements Med.* **10**, 13–15 (1993).

43. K. Geraki, M.J. Farquharson, and D.A. Bradley, X-ray fluorescence and energy dispersive x-ray diffraction for the quantification of elemental concentrations in breast tissue, *Phys. Med. Biol.* **49**, 99–110 (Jan 7 2004).
44. U. Majewska, D. Banas, J. Braziewicz, S. Gozdz, A. Kubala-Kukus, and M. Kucharzewski, Trace element concentration distributions in breast, lung and colon tissues, *Phys. Med. Biol.* **52**, 3895–911 (Jul 7 2007).
45. K. Geraki, M.J. Farquharson, and D.A. Bradley, Concentrations of Fe, Cu and Zn in breast tissue: a synchrotron XRF study, *Phys. Med. Biol.* **47**, 2327–39 (Jul 7 2002).
46. S.L. Rizk and H.H. Sky-Peck, Comparison between concentrations of trace elements in normal and neoplastic human breast tissue, *Cancer. Res.* **44**, 5390–4 (Nov 1984).
47. S. Rizk and H. Sky-Peck, Comparison between Concentrations of Trace Elements in Normal and Neoplastic Human Breast Tissue, *Cancer. Research.* **44**, 5390–539 (1984).
48. P.M. Santoliquido, H.W. Southwick, and J.H. Olwin, Trace metal levels in cancer of the breast, *Surg. Gynecol. Obstet.* **142**, 65–70 (Jan 1976).
49. M. Brys, A.D. Nawrocka, E. Miekos, C. Zydek, M. Foksinski, A. Barecki, and W.M. Krajewska, Zinc and cadmium analysis in human prostate neoplasms, *Biol. Trace. Elem. Res.* **59**, 145–52 (Winter 1997).
50. A. Feustel, R. Wennrich, D. Steiniger, and P. Klaus, Zinc and cadmium concentration in prostatic carcinoma of different histological grading in comparison to normal prostate tissue and adenofibromyomatosis (BPH), *Urol. Res.* **10**, 301–3 (1982).
51. V. Zaichick, T.V. Sviridova, and S.V. Zaichick, Zinc in the human prostate gland: normal, hyperplastic and cancerous, *Int. Urol. Nephrol.* **29**, 565–74 (1997).
52. E. Andrasi, M. Suhajda, I. Saray, L. Bezur, L. Ernyei, and A. Reffy, Concentration of elements in human brain: glioblastoma multiforme, *Sci. Total. Environ.* **139/140**, 399–402 (Nov 1 1993).
53. M. Persigehl, H. Schicha, K. Kasperek, and H.J. Klein, Trace element concentration in human organs in dependence of age, *Beitr. Path.* **161**, 209–220 (1977).
54. E.J. Margalioth, J.G. Schenker, and M. Chevion, Copper and zinc levels in normal and malignant tissues, *Cancer* **52**, 868–72 (Sep 1 1983).
55. P. Ghadirian, P. Maisonneuve, C. Perret, G. Kennedy, P. Boyle, D. Krewski, and A. Lacroix, A case-control study of toenail selenium and cancer of the breast, colon, and prostate, *Cancer. Detect. Prev.* **24**, 305–13 (2000).
56. I. Kato, A.M. Dnistrian, M. Schwartz, P. Toniolo, K. Koenig, R.E. Shore, A. Zele-niuch-Jacquotte, A. Akhmedkhanov, and E. Riboli, Iron intake, body iron stores and colorectal cancer risk in women: a nested case-control study, *Int. J. Cancer.* **80**, 693–8 (Mar 1 1999).
57. R.L. Nelson, F.G. Davis, E. Sutter, L.H. Sobin, J.W. Kikendall, and P. Bowen, Body iron stores and risk of colonic neoplasia, *J. Natl. Cancer. Inst.* **86**, 455–60 (Mar 16 1994).
58. K. Witkowski, A. Kozlowski, M. Pardela, J. Piecuch, and P. Walichewicz, [Level of copper in plasma and tissue of patients with esophageal and large bowel cancer], *Wiad. Lek.* **46**, 586–8 (Aug 1993).
59. K.Q. Xiao and W.J. Henderson, [Electron microscopy microanalysis and quantitative detection of trace elements in carcinoma of the colon], *Zhonghua Bing Li Xue Za Zhi* **21**, 142–5 (Jun 1992).
60. W.P. Banner, J.J. DeCosse, Q.H. Tan, and M.S. Zedeck, Selective distribution of selenium in colon parallels its antitumor activity, *Carcinogenesis* **5**, 1543–6 (Dec 1984).
61. G.C. Gregoriadis, N.S. Apostolidis, A.N. Romanos, and T.P. Paradellis, A comparative study of trace elements in normal and cancerous colorectal tissues, *Cancer* **52**, 508–19 (Aug 1 1983).
62. Z.M. Bataineh, I.H. Bani Hani, and J.R. Al-Alami, Zinc in normal and pathological human prostate gland, *Saudi. Med. J.* **23**, 218–20 (Feb 2002).
63. A. Feustel, R. Wennrich, and H. Dittrich, Investigations of trace elements in metastases and primary carcinoma of the prostate, *Urol. Res.* **17**, 107–9 (1989).

64. J.O. Ogunlewe and D.N. Osegbe, Zinc and cadmium concentrations in indigenous blacks with normal, hypertrophic, and malignant prostate, *Cancer* **63**, 1388–92 (Apr 1 1989).
65. I. Romics and L. Katchalova, Spectrographic determination of zinc in the tissues of adenoma and carcinoma of the prostate, *Int. Urol. Nephrol.* **15**, 171–6 (1983).
66. M. Yaman, D. Atici, S. Bakirdere, and I. Akdeniz, Comparison of trace metal concentrations in malign and benign human prostate, *J. Med. Chem.* **48**, 630–634 (2005).
67. F.K. Habib, G.L. Hammond, I.R. Lee, J.B. Dawson, M.K. Mason, P.H. Smith, S.R.Y.K. Stitch, A.G. Meade, E.P. Rack, and A.J. Blotcky, Metal-androgen interrelationships in carcinoma and hyperplasia of the human prostate, *J. Endocrinol.*, **61** (1), 133–41 (1976).
68. H. Kubo, S. Hashimoto, and A. Ishibashi, Simultaneous determinations of Fe, Cu, Zn, and Br concentrations in human tissue sections, *Med. Phys.* **3**, 204–9 (Jul-Aug 1976).
69. G.M. Brittenham and D.G. Badman, Noninvasive measurement of iron: report of an NIDDK workshop, *Blood* **101**, 15–9 (Jan 1 2003).
70. J.M. Alustiza, J. Artetxe, A. Castiella, C. Agirre, J.I. Emparanza, P. Otazua, M. Garcia-Bengochea, J. Barrio, F. Mujica, and J.A. Recondo, MR quantification of hepatic iron concentration, *Radiology* **230**, 479–84 (Feb 2004).
71. W.F. Avrin and S. Kumar, Noninvasive liver-iron measurements with a room-temperature susceptometer, *Physiol. Meas.* **28**, 349–61 (Apr 2007).
72. H.L. Bonkovsky, R.B. Rubin, E.E. Cable, A. Davidoff, T.H. Rijcken, and D.D. Stark, Hepatic iron concentration: noninvasive estimation by means of MR imaging techniques, *Radiology* **212**, 227–34 (Jul 1999).
73. G.M. Brittenham, S. Sheth, C.J. Allen, and D.E. Farrell, Noninvasive methods for quantitative assessment of transfusional iron overload in sickle cell disease, *Semin. Hematol.* **38**, 37–56 (Jan 2001).
74. E. Cecchin, S. De Marchi, F. Querin, M.G. Marin, R. Fiorentino, and F. Tesio, Efficacy of hepatic computed tomography to detect iron overload in chronic hemodialysis, *Kidney. Int.* **37**, 943–50 (Mar 1990).
75. R.W. Chapman, G. Williams, G. Bydder, R. Dick, S. Sherlock, and L. Kreel, Computed tomography for determining liver iron content in primary haemochromatosis, *Br. Med. J.* **280**, 440–2 (Feb 16 1980).
76. J.L. Chezmar, R.C. Nelson, J.A. Malko, and M.E. Bernardino, Hepatic iron overload: diagnosis and quantification by noninvasive imaging, *Gastrointest. Radiol.* **15**, 27–31 (Winter 1990).
77. R.M. Dixon, P. Styles, F.N. al-Refai, G.J. Kemp, S.M. Donohue, B. Wonke, A.V. Hoffbrand, G.K. Radda, and B. Rajagopalan, Assessment of hepatic iron overload in thalassemic patients by magnetic resonance spectroscopy, *Hepatology* **19**, 904–10 (Apr 1994).
78. Y. Gandon, D. Olivie, D. Guyader, C. Aube, F. Oberti, V. Sebillle, and Y. Deugnier, Non-invasive assessment of hepatic iron stores by MRI., *Lancet* **363**, 357–362 (Jan 31, 2004 2004).
79. D. Guyader, Y. Gandon, J.Y. Robert, J.F. Heautot, H. Jouanolle, C. Jacquelinet, M. Messner, Y. Deugnier, and P. Brissot, Magnetic resonance imaging and assessment of liver iron content in genetic hemochromatosis, *J Hepatol* **15**, 304–8 (Jul 1992).
80. J.M. Howard, C.N. Ghent, L.S. Carey, P.R. Flanagan, and L.S. Valberg, Diagnostic efficacy of hepatic computed tomography in the detection of body iron overload, *Gastroenterology* **84**, 209–15 (Feb 1983).
81. P. Liu, M. Henkelman, J. Joshi, P. Hardy, J. Butany, M. Iwanochko, M. Clauberg, M. Dhar, D. Mai, S. Wai, and N. Olivieri, Quantification of cardiac and tissue iron by nuclear magnetic resonance relaxometry in a nvel murine thalassemia-cardiac iron overload model, *Can. J. Cardiol.* **12**, 155–64 (Feb 1996).
82. P. Nielsen, R. Engelhardt, M. Duerken, G.E. Janka, and R. Fischer, Using SQUID biomagnetic liver susceptometry in the treatment of thalassemia and other iron loading diseases, *Transfus. Sci.* **23**, 257–8 (Dec 2000).

83. P. Nielsen, R. Engelhardt, J. Dullmann, and R. Fischer, Non-invasive liver iron quantification by SQUID-biosusceptometry and serum ferritin iron as new diagnostic parameters in hereditary hemochromatosis, *Blood Cells Mol. Dis.* **29**, 451–8 (Nov-Dec 2002).
84. P. Nielsen, U. Kordes, R. Fischer, R. Engelhardt, and G.E. Janka, [SQUID-biosusceptometry in iron overloaded patients with hematologic diseases], *Klin Padiatr* **214**, 218–22 (Jul-Aug 2002).
85. H. Perrimond, C. Chagnon, I. Moulanier, G. Michel, H. Guidicelli, and P.J. Bernard, The value of nuclear magnetic resonance in the study of iron overload in thalassemia patients, *Ann. Pediatr. (Paris)* **38**, 175–84 (Mar 1991).
86. S. Sheth, SQUID biosusceptometry in the measurement of hepatic iron, *Pediatr. Radiol.* **33**, 373–7 (Jun 2003).
87. D. Vartsky, K.J. Ellis, D.M. Hull, and S.H. Cohn, Nuclear resonant scattering of gamma rays – a new technique for in vivo measurement of body iron stores, *Phys. Med. Biol.* **24**, 689–701 (Jul 1979).
88. D. Vartsky, L. Wielopolski, K.J. Ellis, and S.H. Cohn, The Use of Nuclear Resonant Scattering of Gamma-Rays for In vivo Measurement of Iron, *Nucl. Instrum. Meth. Phys. Res.* **193**, 359–364 (1982).
89. E. Angelucci, A. Giovagnoni, G. Valeri, E. Paci, M. Ripalti, P. Muretto, C. McLaren, G. M. Brittenham, and G. Lucarelli, Limitations of magnetic resonance imaging in measurement of hepatic iron, *Blood* **90**, 4736–42 (Dec 15 1997).
90. Z.J. Wang, J.C. Haselgrove, M.B. Martin, A.M. Hubbard, S. Li, K. Loomes, J.R. Moore, H. Zhao, and A.R. Cohen, Evaluation of iron overload by single voxel MRS measurement of liver T2, *J. Magn. Reson. Imaging* **15**, 395–400 (Apr 2002).
91. A.J. Kapadia, A.C. Sharma, G.D. Tourassi, J.E. Bender, A.S. Crowell, M.R. Kiser, C.R. Howell, and C.E. Floyd, Neutron Spectroscopy of Mouse Using Neutron Stimulated Emission Computed Tomography (NSECT), in *IEEE Nuclear Science Symposium, Medical Imaging Conference*, San Diego, CA, pp. 3546–3548 (2006).
92. A.C. Sharma, G.D. Tourassi, A.J. Kapadia, A.S. Crowell, M.R. Kiser, A. Hutcheson, B. P. Harrawood, C.R. Howell, and C.E. Floyd, Elemental Spectrum of a Mouse Obtained via Neutron Stimulation., in *2007 SPIE Symposium on Medical Imaging*, San Diego, CA, p. 65100 K (2007).
93. C.E. Floyd, A.C. Sharma, J.E. Bender, A.J. Kapadia, J.Q. Xia, B.P. Harrawood, G.D. Tourassi, J.Y. Lo, M.R. Kiser, A.S. Crowell, R.S. Pedroni, R.A. Macri, S. Tajima, and C. R. Howell, Neutron Stimulated Emission Computed Tomography: Background Corrections, *Nucl. Instrum. Meth. Phys. Res. Sect. B* **254**, 329–336 (2007).
94. C.E. Floyd, A.J. Kapadia, J.E. Bender, A.C. Sharma, J.Q. Xia, B.P. Harrawood, G.D. Tourassi, J.Y. Lo, A.S. Crowell, M.R. Kiser, and C.R. Howell, Neutron Stimulated Emission Computed Tomography of a Multi-Element Phantom, *Phys. Med. Biol.* **53**, 2313–2326 (2008).
95. K. Lange and R. Carson, EM reconstruction Algorithms for Emission and Transmission Tomography, *Journal of Computer Assisted Tomography* **8**, 306–316 (1984).
96. A.J. Kapadia, Accuracy and Patient Dose in Neutron Stimulated Emission Computed Tomography for Diagnosis of Liver Iron Overload: Simulations in GEANT4, in *Biomedical Engineering*, vol. PhD, Duke University, Durham, NC (2007).
97. W.A. Watson, III, J. Chen, G. Heyes, E. Jastrzembski, and D. Quarrie, CODA: a scalable, distributed data acquisition system, in *IEEE Transactions on Nuclear Science*, Vancouver, BC, Canada, pp. 61–68 (1994).
98. R. Fox, C. Bolen, K. Orji, and J. Venema, NSCLSpecTcl Meeting the Needs of Preliminary Nuclear Physics Data Analysis in *11th Annual Tcl/Tk Conference* New Orleans, Louisiana (2004).
99. RSNA, Radiation Exposure in X-ray Examinations, in *American College of Radiology (ACR) and the Radiological Society of North America (RSNA)* (2007).

100. A.C. Sharma, B.P. Harrawood, J.E. Bender, G.D. Tourassi, and A.J. Kapadia, Neutron stimulated emission computed tomography: a Monte Carlo simulation approach, *Phys. Med. Biol.* **52**, 6117–31 (Oct 21 2007).
101. J.E. Bender, A.J. Kapadia, A.C. Sharma, G.D. Tourassi, B.P. Harrawood, and C. E. Floyd, Breast cancer detection using Neutron Stimulated Emission Computed Tomography: prominent elements and dose requirements, *Med. Phys.* **34**, 3866–3871 (2007).
102. A.J. Kapadia, C.E. Floyd, C.R. Howell, and B.P. Harrawood, Sampling Requirements for Neutron Stimulated Emission Computed Tomography, in *RSNA, Physics (Digital Imaging, PACS) session* Chicago, IL (2004).